International Journal of Nanoelectronics and Materials
IJNeaM
ISSN 1985-5761 | E-ISSN 2232-1535

Comparative Evaluation of CTAB and AP1 Buffers in On-Chip DNA Extraction of Pathogenic Fungus for Microfluidic Interdigitated-Electrode Biosensing

Adilah Ayoib[a,b,c,*], Shahidah Arina Shamsuddin[b,d], Nor Azizah Parmin[b], and Rajapaksha Dewage Asanka Amith Rajapaksha[e]

[a]*Faculty of Chemical Engineering & Technology, Universiti Malaysia Perlis (UniMAP), Arau 02600, Malaysia*
[b]*Institute of Nano Electronic Engineering, Universiti Malaysia Perlis (UniMAP), Kangar 01000, Malaysia*
[c]*Carbon Sustainability Nexus (CaSNex), Special Interest Group (SIG), Universiti Malaysia Perlis (UniMAP), Arau 02600, Malaysia*
[d]*Faculty of Mechanical Engineering & Technology, Universiti Malaysia Perlis (UniMAP), Padang Besar 02100, Malaysia*
[e]*Department of Nano Science Technology, Faculty of Technology, Wayamba University of Sri Lanka, Kuliyapitiya 60200, Sri Lanka*
** Corresponding author. Tel.: +6013-509-2811; e-mail: adilahayoib@unimap.edu.my*

Received 15 September 2023, Revised 1 October 2025, Accepted 27 October 2025

ABSTRACT

Conventional methods such as tissue culture and PCR-based analyses are expensive and time-consuming, often requiring up to two weeks and intensive labor. In contrast, microfluidic lab-on-a-chip systems provide much faster detection (roughly an hour), reduce costs, and require only minimal sample volumes. This study presents a streamlined PDMS microfluidic workflow for on-chip DNA extraction and label-free detection of *Ganoderma boninense,* a pathogenic fungus that majorly impacts palm oil plantations in Malaysia. We compared two lysis buffers, CTAB and AP1, to evaluate DNA yield and purity. UV-Vis analysis indicated that AP1 consistently resulted in higher DNA concentrations, while CTAB extracts exhibited smoother absorbance spectra, suggesting lower levels of impurities. In addition to that, the expected peak near 260 nm was observed with additional shoulders around 280–290 nm across extracts, which are characteristic of both dsDNA and ssDNA, demonstrating successful DNA extraction on the microfluidics chip. Electrical I-V measurements using the AuNP-ZnO-coated IDE biosensor revealed increased DNA hybridization signals, confirming both extraction and detection processes were successful. Overall, AP1 produced a much higher DNA recovery (albeit with increased background absorbance), whereas CTAB yielded 'purer' DNA. This integrated microfluidic system enables rapid and sensitive detection of *G. boninense*, demonstrating its potential for field-based diagnostic applications.

Keywords: *DNA extraction, PDMS, Microfluidics, Biosensor, Lab-on-a-chip*

1. INTRODUCTION

Ganoderma boninense is a soil-borne fungal pathogen that causes basal stem rot (BSR), a severe disease affecting oil palm plantations in Malaysia and surrounding regions [1]. BSR can infect young palms asymptomatically, which, in turn, leads to devastating yield losses. This problem highlights the necessity for early and reliable detection methods. Conventional diagnostics, such as tissue culture and molecular analyses are costly and time-consuming, often taking weeks to yield results. In comparison, microfluidic integrating lab-on-a-chip (LOC) biosensors streamlines sample preparation and detection in one platform using minimal sample volumes for faster and lower-cost analysis [2], [3], [4]. Table 1 shows some microfluidic applications across various pathogens and sample types in the last decade.

Compared to these, our platform integrates on-chip chemical lysis and DNA extraction with label-free electrical hybridization detection. This approach eliminates the need for magnetic beads and amplification, reduces reagent consumption, and accelerates the overall assay relative to current systems, achieving a simplified single-step workflow of approximately 1 hour.

Our paper presents the development of a single-channel polydimethylsiloxane (PDMS) microfluidic chip integrated with a functionalized interdigitated-electrode (IDE) biosensor for on-chip analysis. Cetyltrimethyl-ammonium bromide (CTAB) buffer, which is commonly used for fungal lysis due to its effectiveness in removing polysaccharides and phenolics, and the commercial AP1 buffer (Qiagen®, Germany), which contains polyvinylpyrrolidone/dithio-threitol (PVP/DTT) to enhance DNA yield in polyphenolic-rich fungal matrices, were used for evaluation of lysis chemistries. The application of an appropriate lysis buffer is critical for optimal on-chip DNA extraction outcomes.
This proof-of-concept (Figure 1) integrates microfluidic engineering with molecular diagnostics, paving the way for rapid *G. boninense* detection in agricultural settings. The outcomes of this study could significantly enhance disease management strategies and contribute to sustainable oil palm cultivation.

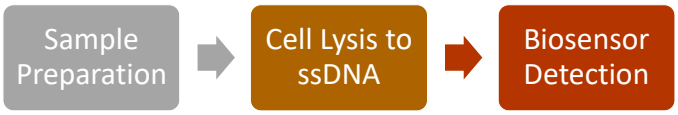

Figure 1. Overview of DNA extraction on a LOC system.

Table 1 Advances in Microfluidic DNA Extraction and Detection Over the Past Decade

No.	Microfluidic System	Extraction Method	Key Results	Ref.
1.	Thermally-actuated IFAST chip (stool interface)	Chaotropic lysis + dried magnetic particles (PMPs)	Rapid DNA release and binding in 7 min from crude stool; 40× volume concentration; platform for POC DNA prep	[5]
2.	Automated chip with magnet-actuation (environmental samples)	Thermal/chemical/enzymatic cell lysis + magnetic-particle purification	LOD ≈10^2–10^3 genome/mL in water, 1–10 GE/10L in air; detected Campylobacter DNA in farm air samples	[6]
3.	Integrated PCR/LAMP lab-on-chip (Fraunhofer prototype)	On-chip cell lysis (with optional magnetic bead DNA extraction)	Proof-of-concept multiplex pathogen test: on-chip bacterial isolation, lysis, DNA extraction, amplification (LAMP/PCR) for *E. coli* and *Salmonella* detection	[7]
4.	Polymer/paper "IPμchip" platform (portable)	On-chip magnetic-bead DNA extraction	15 min extraction vs >90 min manual; LAMP amplification of *S. pneumoniae/M. pneumoniae* to 20 fg sensitivity; smartphone readout, point-of-care multiplex detection	[8]
5.	Finger-actuated microfluidic biosensor	Immuno-magnetic capture + silica-coated MNP DNA absorption	"Sample-in-answer-out" *E. coli* O157:H7 assay; RPA-CRISPR/Cas12a detection, LOD 10 CFU/mL, range 10^2–10^8 CFU/mL in 2.5 h; recovery 104–120%	[9]
6.	PDMS-based microfluidic chip fabricated using SU-8 photoresist on glass substrate	Automated, high-throughput DNA extraction protocol integrated with a label-free biosensor	Achieved DNA extraction and detection of *G. boninense* within 2 hours; UV-Vis, FTIR, and PCR confirmed effectiveness; device showed ≤0.1 mm fabrication tolerance.	[10]
7.	Portable lab-on-chip device utilizing magnetic beads	Modified on-chip DNA extraction methodology	Enabled DNA extraction of *G. boninens* in ~15 minutes; PCR validation showed comparable performance to benchtop protocols; system accommodated two samples of 120 μL	[11]
8.	Integrated microfluidic cfDNA chip	Vortex micromixer + magnetic beads with capture probes	76% cfDNA recovery (200 μL plasma) in 45 min; on-chip allele-specific qPCR for *BRCA1* mutations in 90 min; enables automated screening for cancer biomarkers	[12]
9.	Handheld capillary LAMP chip	Microneedle DNA extraction (on-chip)	Colorimetric LAMP on chip for meat species authentication; pricking meat with microneedle releases DNA; 6 meat species distinguished; detection of 1% adulteration in 60 min; cost <$1 per test	[13]
10.	Rotating-cartridge POCT PCR platform	Integrated cartridge with lyophilized reagents (encapsulated extraction reagents)	Simultaneous 6-plex virus testing (HPV, SARS-CoV-2, etc.) in 1 h; LOD 1000 copies/mL for HPV, 200 copies/mL for SARS-CoV-2; 100% sensitivity, >98% specificity in clinical samples	[14]
11.	μPAD LAMP-CRISPR platform	Magnetic silica beads (tube extraction) + on-chip LAMP & CRISPR/Cas12a	A portable device (syringe & tubing) integrates magnetic bead DNA extraction with LAMP-CRISPR. Total assay ~1 h; detected *Salmonella* at 10^2 CFU/mL in food samples; visual readout via smartphone; high specificity	[15]
12.	Microfluidic qPCR array	Off-chip extraction, on-chip qPCR	Multiplex qPCR chip for 21 respiratory viruses from clinical swabs; detected ≥1 virus in 76.6% of samples (n=158), including rhinovirus, adenovirus, etc.; demonstrated high-throughput surveillance capability	[16]
13.	Integrated PMMA POCT chip	Adsorption on magnetic nanoparticles	SARS-CoV-2 sample-to-answer: 5 min load, 3 min magnetic bead RNA extraction, 20 min RT-LAMP (total 28 min); LOD <297 copies; cost ≈$9.5 per test; performance comparable to benchtop kits	[17]

14.	Pressure-driven micro-chamber array	On-chip spheroplast lysis	Extraction of intact bacterial chromosomes: a single *B. subtilis* genome isolated in a microfluidic chamber (lysing in situ). DNA was deproteinized on-chip, demonstrated genome release and addition of exogenous factors for genome-in-a-box studies	[18]
15.	Gravity-driven microcapillary siphon array	Magnetic bead (silica) DNA binding in capillaries	Bacterial DNA extraction from complex matrices (blood, water): using 10×200 µm capillaries and external magnet; achieved >90% recovery vs 52% manual; linear qPCR detection of *E. coli* in buffer, blood, river water; reusable chip with no cross-contamination	[19]
16.	Multiplex CRISPR microfluidic chip	Off-chip RPA amplification + on-chip CRISPR-Cas12a	"Space-coded" chip partitions RPA amplicons for 9 respiratory viruses (influenza A/B, 4 coronaviruses, RSV, etc.) in one run; detection <40 min; LOD ~1 copy/reaction (10^−18 M); tested on 35 patient samples: 90% sensitivity, 100% specificity	[20]

2. METHODOLOGY

2.1. Design and Fabrication of Microfluidic Chip

The microfluidic chip is fabricated using a two-stage process: first, a master template is created with SU-8, followed by the replication of PDMS on a microscope glass substrate for low-cost fabrication, as previously described in our papers [21], [22]. Briefly, an AutoCAD-designed photomask was printed on high-resolution transparency and used to pattern SU-8 photoresist on a glass substrate via photolithography. The resulting SU-8 master mold was coated with PDMS, cured, and peeled off. Inlet and outlet holes were punched into the PDMS, which was then plasma-bonded to a new glass slide to form sealed microfluidic channels. Figure 2 illustrates this process.

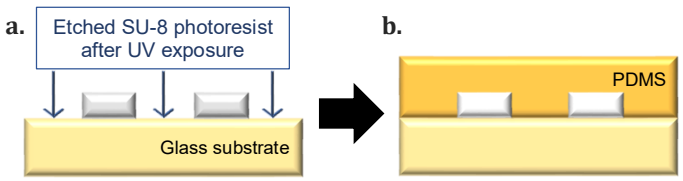

Figure 2. The two-stage fabrication of PDMS microfluidics. (a) Development of an SU-8 master template via the photolithography process. (b) Plasma bonding of a PDMS replicate on a glass substrate to create microfluidic channels after the soft lithography process.

2.2. Fungal Growth and Cultivation

G. boninense cultures were grown in potato dextrose broth (PDB) at room temperature (30°C ± 2) and 250 rpm for 12 days. A 0.5 mL aliquot was then transferred onto potato dextrose agar (PDA) plates and incubated for one additional week to generate fresh hyphae. These fungal mycelia were used for downstream DNA extraction Figure 3.

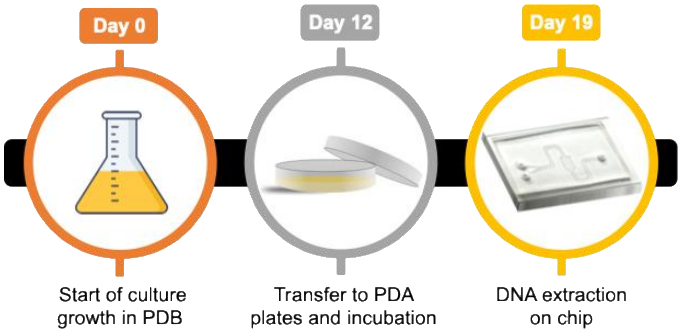

Figure 3. Schematic illustration of fungal cultivation for DNA extraction on a microfluidic chip.

2.3. Preparation of Lysis Buffers and DNA Extraction On-Chip

Two lysis buffers were prepared for on-chip extraction [10]: a CTAB-based buffer (100 mM Tris-HCl pH 8.4, 1.4 M NaCl, 25 mM EDTA, 2% CTAB) preheated to 65°C, and AP1 buffer (10 mM Tris-HCl pH 8.0, 1 mM EDTA, 0.1% SDS, 0.1 M NaCl, 1× PVP, 10 mM DTT) used at room temperature. Each buffer was supplemented immediately before use with 5 mg/mL proteinase K and 50 µg/mL RNase A. We infused these lysis solutions into the chip to lyse cells and release DNA. DNA extracts were collected from the outlet at three time points: immediately, 4 hours later, and after overnight incubation. Samples collected without added NaOH yielded double-stranded DNA (dsDNA), whereas adding NaOH produced single-stranded DNA (ssDNA). All samples and synthetic

DNA controls were analyzed by UV-Vis spectrophotometry to assess DNA yield and purity.

2.4. Molecular and Electrical Characterization of DNA Using UV-Vis Spectroscopy and Functionalized Interdigitated Electrode Biosensor Measurements

The extracted DNA samples were analyzed by UV-Vis spectrophotometry (PerkinElmer) to quantify DNA concentration and assess purity based on the 260 nm absorbance peak. Electrical characterization was performed on a functionalized IDE biosensor designed and fabricated as previously described [23], [24] (Keithley 2200 SMU, USA). The IDE surface was coated with zinc oxide and gold nanoparticles (AuNPs) (30 nm) (Sigma Aldrich, USA) to enhance conductivity. A thiolated *G. boninense* ssDNA probe was immobilized on the AuNP-coated IDE, forming a specific recognition layer. Target DNA extracts were applied to the biosensor, and current-voltage (0–1 V) curves were recorded to detect hybridization. We compared I–V responses between devices with and without the AuNPs coating to evaluate the hybridization signal.

3. RESULTS AND DISCUSSION

3.1. PDMS Chip Morphology

After fabrication, the SU-8 master mold and PDMS channel were imaged under low-power microscopy (S-EYE software) (Figure 3). Measured dimensions (Table 2) matched the design specifications. Assembly of the transparency print, master mold, and final PDMS chip is shown in Figure 4. Water flow tests showed no leakage, confirming the integrity of the plasma-sealed channel.

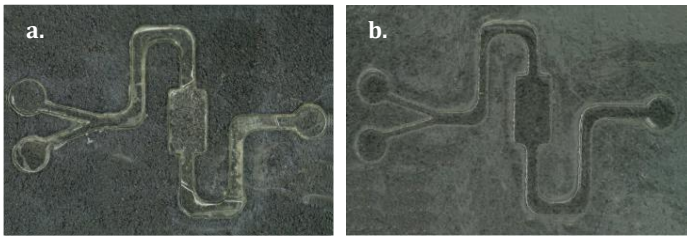

Figure 3. Images of the fabricated microfluidic chip under low-power microscopy (a) SU-8 master template (b) PDMS replicate.

Table 2 Size and dimension of the microfluidic chip design on AutoCAD software

Design	Dimension (mm)
Inlet width	0.5
Inlet radius	1.4
Outlet width	1.0
Outlet radius	1.3
Cell-capture width × length	3.0 × 5.0

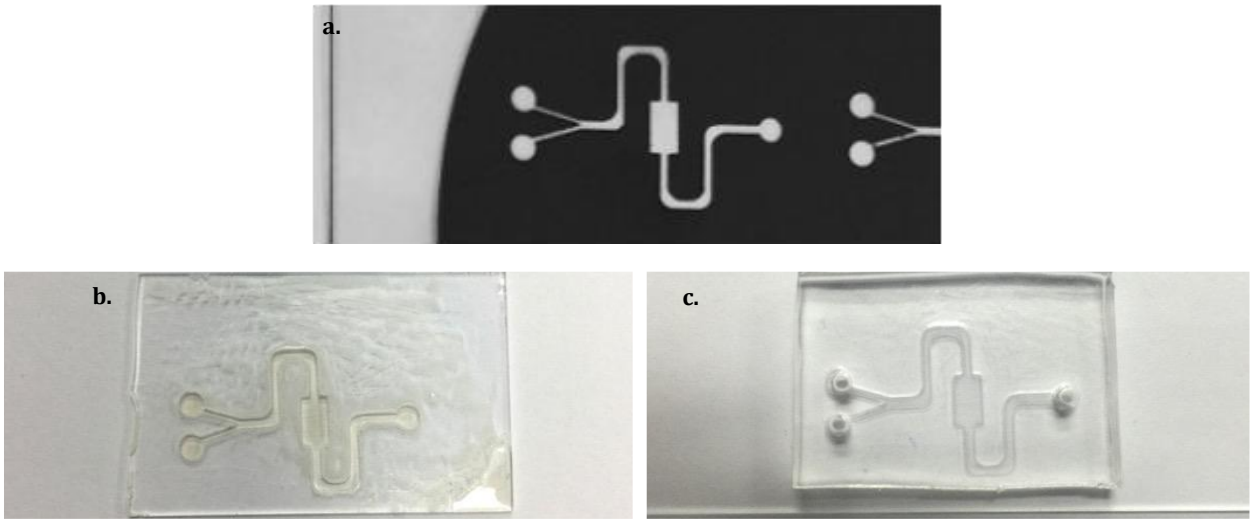

Figure 4. Images of the microfluidic chip at its initial and completed stages. (a) Printed design of the microfluidic chip on transparency. (b) Fabricated microfluidic SU-8 master template. (c) Fully assembled microfluidic chip ready for DNA extraction.

3.2. UV-Vis Vis Analysis on CTAB and AP1 Methods of DNA Extraction on Microfluidic Chip

The UV-Vis spectra of DNA extracts, shown in Figures 5 and 6, reveal the absorbance characteristics of outlet samples collected at different time intervals. Pure DNA typically exhibits a peak near 260 nm [3], [23], [24], [25], as demonstrated by the synthetic control in both figures. In contrast, raw sample absorbance (negative control) exhibits very low absorbance (<0.05 A) and is negligible. Both extraction methods confirmed the presence of DNA, although AP1 extracts, as seen in Figure 6, are shown to produce significantly higher concentrations compared to CTAB extracts (Figure 5), as indicated by elevated A260 absorbance values (Table 3).

Table 3 DNA concentration and purity at different sampling times

Sample	A260	A260/ A280	A260/ A230
Synthetic ssDNA	2.31	1.54	1.16
ssDNA CTAB immediately	1.39	1.70	0.14
ssDNA CTAB after 4 hours	2.23	1.84	0.54
ssDNA CTAB overnight	3.16	2.01	0.32
ssDNA AP1 immediately	3.03	1.47	0.97
ssDNA AP1 after 4 hours	3.54	1.81	0.35
ssDNA AP1 overnight	3.53	1.49	1.05

The improved DNA recovery from AP1 extracts can be attributed to the inclusion of PVP in the AP1 buffer, which binds polyphenolic inhibitors via hydrogen bonding [26], facilitating DNA extraction from crude fungal lysates. CTAB extracts, by comparison, yielded smoother spectra with lower baseline noise (Figure 5), which is an indication of reduced impurity interference. The shift in the absorbance peak may suggest the presence of additional molecules alongside DNA, while minor shoulders near 230 nm in both extraction methods suggest residual salts or phenolic compounds, particularly in the CTAB extracts. And thus, even though AP1 lysis yielded a greater quantity of DNA, CTAB lysis can be said to produce comparatively 'purer' DNA.

Analysis of absorbance ratios A260/A280 and A260/A230 served as secondary indicators of DNA purity (Table 3). Generally, an A260/A280 ratio between 1.7 and 1.9 is indicative of relatively pure DNA. The synthetic ssDNA control exhibited an A260 of 2.3 and an A260/A280 ratio of 1.54. AP1-extracted samples frequently exceeded 3.0 OD units at 260 nm, indicating highly concentrated DNA that may surpass the spectrophotometer's linear range. CTAB-extracted samples exhibited lower A260 values and A260/A280 ratios of 1.7–2.0, suggesting lower levels of co-extracted contaminants or salts. After 4 hours, both AP1 and CTAB samples showed A260/A280 values of 1.8, supporting the suitability of this time point for DNA analysis.

It is well established that pH variations can significantly influence absorbance ratios [27], [28]. Acidic conditions tend to decrease the A260/A280 ratio by 0.2–0.3 units, while alkaline conditions may increase it comparably. The A260/A230 ratio for pure DNA, which ranges between 2.0–2.2, is sensitive to the presence of contaminants such as proteins, polysaccharides, phenolics, chaotropic salts, and buffer components. In this study, all measured A260/A230 ratios fell below the conventional purity threshold. One possible explanation for this is most likely due to the use of deionized water as the spectrophotometric blank when DNA samples were suspended in Tris-EDTA (TE) buffer. The differences in ionic strength and pH between the blank and the DNA samples are what probably contributed to absorbance shifts, resulting in artificially lowered purity ratios. Additionally, residual NaOH from the ssDNA generation process may have introduced minor pH inconsistencies that affected absorbance measurements.

Apart from that, the elevated A260 values observed in actual DNA extracts compared to the synthetic standard suggest that other nucleic acid species such as RNA or free nucleotides may have contributed to the total absorbance. This is consistent with the use of a chip-based extraction protocol that did not include purification or cleanup steps beyond cell lysis, which limits its ability to produce DNA of high purity. It is important to note, however, that DNA purity assessment was not the primary purpose of this study. Rather, the main objective was to establish a label-free detection approach using a biosensor chip, meaning that the ability to detect the presence of DNA was sufficient for the study's aims.

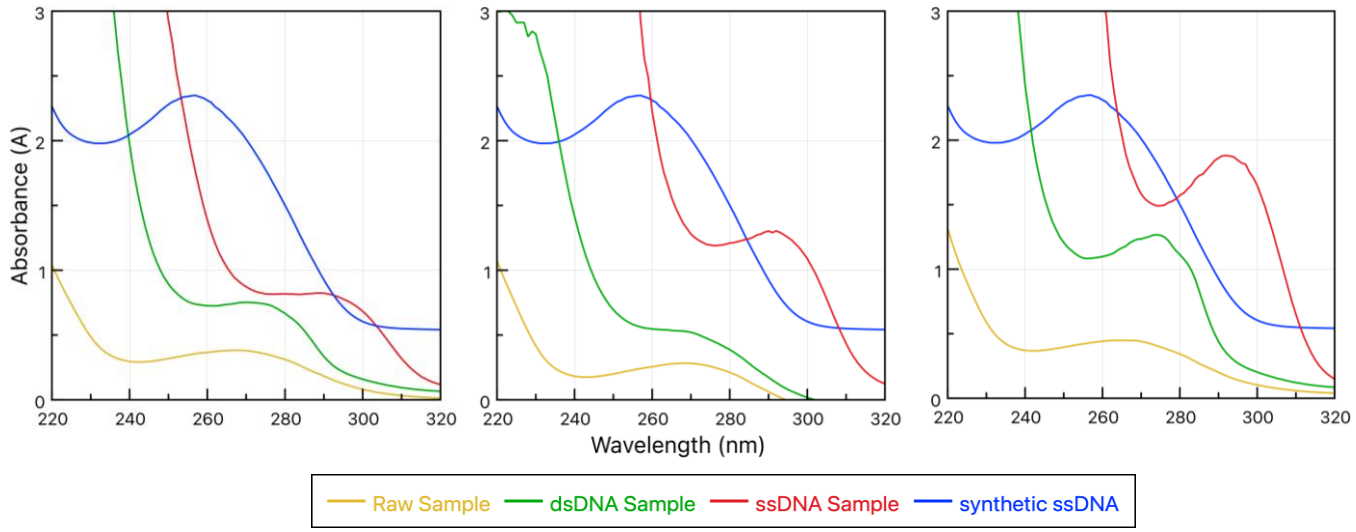

Figure 5. UV-Vis Spectroscopy of *G. boninense* DNA extract using the CTAB method at different time intervals. (a) immediately; (b) after 4 hours; (c) overnight.

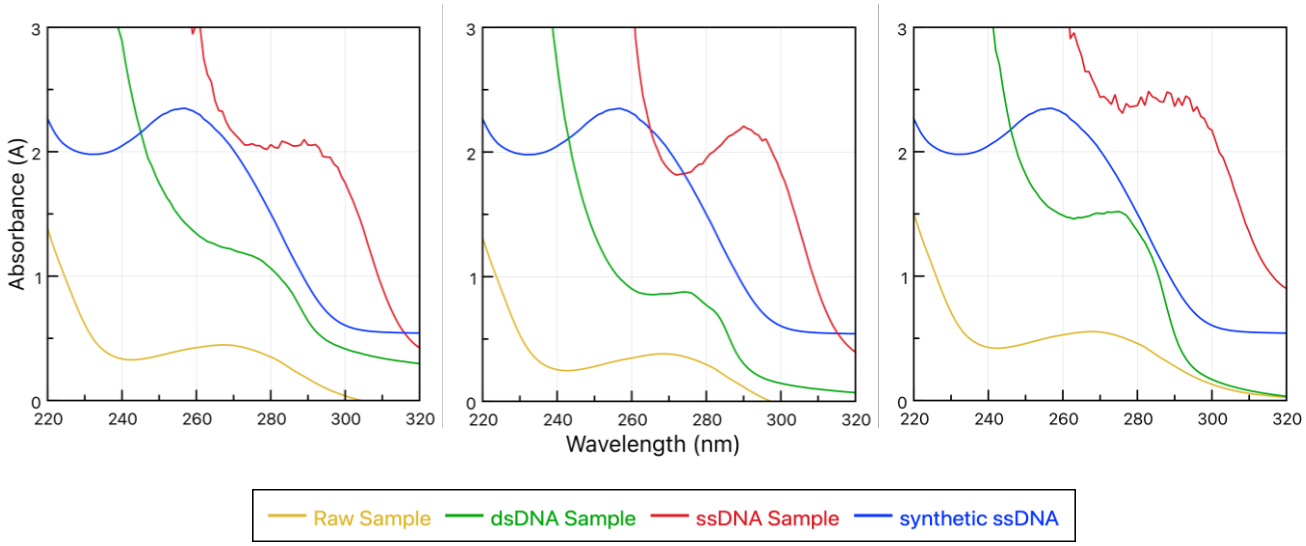

Figure 6. UV-Vis Spectroscopy of *G. boninense* DNA extract using the AP1 method at different time intervals. (a) immediately; (b) after 4 hours; (c) overnight.

Furthermore, spectral shoulders near 230 nm observed with both extraction methods can likely be attributed to buffer components, such as EDTA, or carbohydrate impurities that are common in fungal samples. While CTAB-based methods are well-established for precipitating DNA through high salt concentrations and detergent action, they are also known to co-extract polysaccharides and phenolic compounds unless followed by additional purification steps. In contrast, the PVP containing AP1 buffer appears more effective in reducing such contamination and therefore, enhances DNA yield. This distinction clarifies why AP1 lysis extracts exhibited higher absorbance and concentration values, even though CTAB extracts appeared spectrally 'cleaner'.

All in all, the results from this study align with expectations for label-free chip-based extraction methods suited for single-use detection, highlighting the effectiveness of the AP1 buffer chemistry in producing DNA extracts suitable for downstream applications. It can be noted for this study that the DNA extraction was able to be completed within an hour.

3.3. DNA Detection on Functionalized Biosensor

Electrical characterization was performed by measuring current–voltage (I-V) on the functionalized IDE biosensor to evaluate current flow and changes in electrode connectivity before and after DNA hybridization. As seen in Figures 7 and 8, non-hybridized probes produced a negligible, near-zero current. The immobilized probe DNA, which served as a negative control in both with and without AuNAP-coating exhibited significantly higher currents than both real and synthetic ssDNA at 1.0 V, likely reflecting changes in resistance following the immobilization process.

In an IDE biosensor designed for DNA detection, immobilizing probe DNA and subsequent hybridization with target DNA will result in distinct changes in the system's electrochemical properties. This is because during immobilization, probe ssDNA is covalently attached to the IDE surface, leading to a modest increase in surface charge density and enhanced ionic conductivity in the sensing medium. This in turn, results in higher current as counterions readily diffuse to balance the negatively charged phosphate backbones of the probe ssDNA [29] and maintain high ionic mobility at the electrode surface. Upon hybridization, complementary target DNA binds to the probe, forming dsDNA. This process increases the density of phosphate groups at the electrode-solution interface, further amplifying the negative charge [30], [31]. However, the higher charge density impedes ionic mobility in the electrical double layer due to electrostatic repulsion and the bulkier structure of dsDNA. As a result, the current can often decrease after hybridization. In addition, hybridization modifies the dielectric properties of the interface, as the less flexible dsDNA obstructs ion diffusion and increases resistance. These combined effects may lead to a measurable reduction in current, which forms the basis for signal detection in electrochemical biosensors.

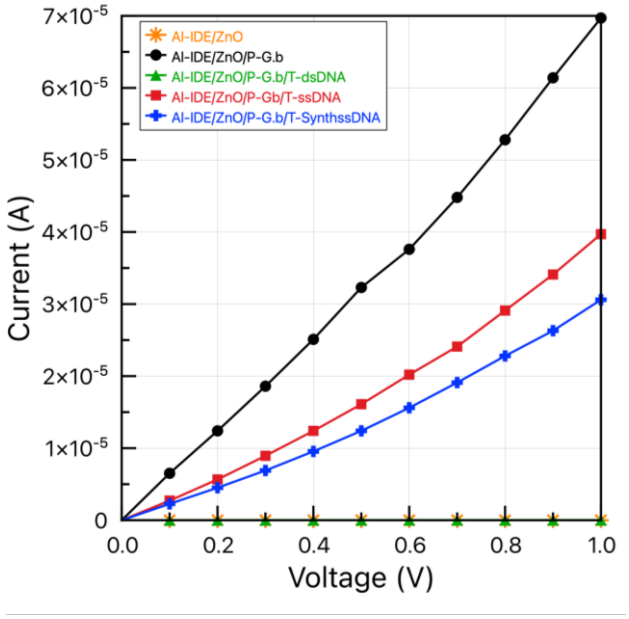

Figure 7. Electrical characterization of *G. boninense* DNA extract without AuNP coating. Al: Aluminum; IDE: Interdigitated Electrode; ZnO: Zinc oxide; AuNPs: Gold nanoparticles; P-G.b: Probe DNA immobilization of G. boninense; T-dsDNA: Target hybridization of dsDNA real sample (non-complementary); T-ssDNA: target hybridization of ssDNA real sample (complementary); T-SynthessDNA: target hybridization of synthetic ssDNA sample (complementary).

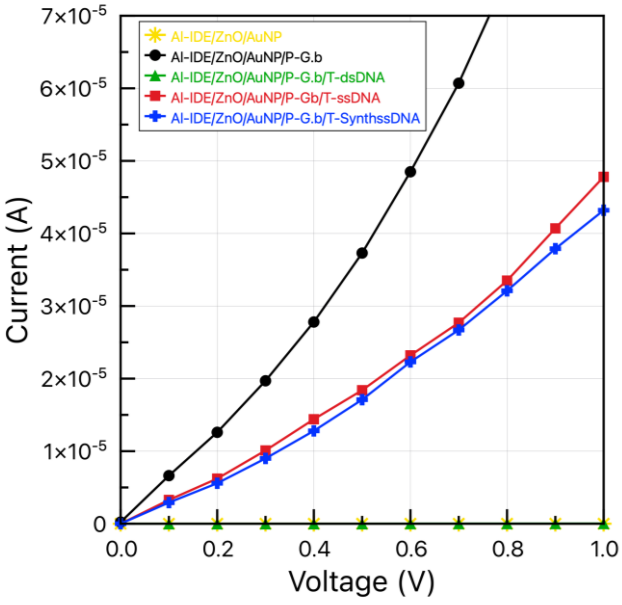

Figure 8. Electrical characterization of *G. boninense* DNA extract with AuNPs coating. Al: Aluminum; IDE: Interdigitated Electrode; ZnO: Zinc oxide; AuNPs: Gold nanoparticles; P-G.b: Probe DNA immobilization of G. boninense; T-dsDNA: Target hybridization of dsDNA real sample (non-complementary); T-ssDNA: target hybridization of ssDNA real sample (complementary); T-SynthessDNA: target hybridization of synthetic ssDNA sample (complementary).

The addition of complementary target DNA caused a substantial current increase in both AuNP-coated and non-AuNP-coated IDEs (Figure 7. Al-IDE/ZnO/P-G.b/T-ssDNA, and Figure 8. Al-IDE/ZnO/AuNP/P-G.b/T-ssDNA), confirming hybridization. Non-complementary control samples, Figure 7. Al-IDE/ZnO/P-G.b/T-dsDNA, and Figure 8. Al-IDE/ZnO/AuNP/P-G.b/T-dsDNA, showed current change nearly equivalent to zero, consistent with their roles as negative controls (no target to hybridize, hence no positive charge carriers). The real (higher-concentration) sample generated a larger current compared to the synthetic standard, consistent with more hybridization, though the values are lower than those observed for the immobilized probe DNA.

Additionally, the AuNP-coated IDE (Figure 8) consistently exhibited higher current responses compared to the non-AuNP-coated IDE (Figure 7), reflecting its enhanced conductivity. The incorporation of AuNPs not only improved the reproducibility of the IDE sensor but also raised the detection threshold for current, attributed to their exceptional chemical stability and biocompatibility [32]. In addition to that, Au facilitates bond formation between the inorganic sensor surface and organic DNA due to its negative charges. Our findings demonstrate that the IDE sensor integrated with AuNPs produces a higher current than the sensor without Au-coating, aligning with the expected electrical characteristics associated with the presence of an additional layer of gold metal oxide. Hence, the overall results for I–V show validation of successful on-chip DNA extraction and hybridization.

4. CONCLUSION

As a proof-of-concept, we demonstrated a PDMS microfluidic LOC system for on-chip extraction and detection of *G. boninense* DNA. Our results showed higher DNA yield extracted from the AP1 buffer lysis while CTAB gave cleaner extracts. The higher DNA yield from AP1 that may have resulted from optimum hybridization led to stronger sensor signals, making AP1 preferable (although CTAB extracts have also hybridized successfully). Integrating on-chip DNA extraction with a label-free IDE biosensor enables rapid (hour-scale) and sensitive detection of the fungal pathogen. This approach significantly reduces sample preparation time compared to conventional methods, suggesting potential for point-of-care or field diagnostics. For future works, we will consider refining buffer formulations and chip design to further improve DNA purity, yield, and sensor performance. Our interdisciplinary platform demonstrates the potential of applying microfluidic biosensors for early *G. boninense* detection in agricultural settings.

ACKNOWLEDGMENTS

The author, 'Adilah Ayoib, gratefully acknowledges support from the Institute of Nano Electronic Engineering and the Faculty of Chemical Engineering & Technology at Universiti Malaysia Perlis (UniMAP), as well as collegues at the Malaysian Palm Oil Board (MPOB). This work was supported by the NanoMalaysia Institute for Innovative Technology (NanoMite), Grant 9012 00006, funded by the Long-Term Research Grant (LRGS) from the Ministry of Education, Malaysia. All views expressed in this publication reflect the author's interpretation of the data and do not necessarily represent those of the funding agencies.

REFERENCES

[1] L. Zakaria, "Basal Stem Rot of Oil Palm: The Pathogen, Disease Incidence, and Control Methods," *Plant Dis*, vol. 107, no. 3, pp. 603–615, Mar. 2023, doi: 10.1094/PDIS-02-22-0358-FE.

[2] S. W. Dutse and N. A. Yusof, "Microfluidics-based lab-on-chip systems in DNA-based biosensing: An overview," *Sensors*, vol. 11, no. 6, pp. 5754–5768, 2011, doi: 10.3390/s110605754.

[3] A. Ayoib, U. Hashim, S. C. B. Gopinath, and M. K. Md Arshad, "DNA extraction on bio-chip: history and preeminence over conventional and solid-phase extraction methods," *Appl Microbiol Biotechnol*, vol. 101, no. 22, pp. 8077–8088, Nov. 2017, doi: 10.1007/s00253-017-8493-0.

[4] J. J. Agrestia *et al.*, "Ultrahigh-throughput screening in drop-based microfluidics for directed evolution," *Proceedings of the National Academy of Sciences*, vol. 107, no. 14, pp. 6550–6550, 2010, doi: 10.1073/pnas.1002891107.

[5] O. Mosley *et al.*, "Sample introduction interface for on-chip nucleic acid-based analysis of Helicobacter pylori from stool samples," *Lab Chip*, vol. 16, no. 11, pp. 2108–2115, 2016, doi: 10.1039/C6LC00228E.

[6] S. Julich *et al.*, "Evaluation of a microfluidic chip system for preparation of bacterial DNA from swabs, air, and surface water samples," *Biologicals*, vol. 44, no. 6, pp. 574–580, Nov. 2016, doi: 10.1016/j.biologicals.2016.06.013.

[7] N. Sandetskaya *et al.*, "An Integrated Versatile Lab-On-A-Chip Platform for the Isolation and Nucleic Acid-Based Detection of Pathogens," *Future Sci OA*, vol. 3, no. 2, May 2017, doi: 10.4155/fsoa-2016-0088.

[8] H. Wang *et al.*, "A versatile loop-mediated isothermal amplification microchip platform for Streptococcus pneumoniae and Mycoplasma pneumoniae testing at the point of care," *Biosens Bioelectron*, vol. 126, pp. 373–380, Feb. 2019, doi: 10.1016/j.bios.2018.11.011.

[9] Y. Shang, G. Xing, X. Liu, H. Lin, and J.-M. Lin, "Fully Integrated Microfluidic Biosensor with Finger Actuation for the Ultrasensitive Detection of *Escherichia coli* O157:H7," *Anal Chem*, vol. 94, no. 48, pp. 16787–16795, Dec. 2022, doi: 10.1021/acs.analchem.2c03686.

[10] A. Ayoib, U. Hashim, and S. C. B. S. C. B. Gopinath, "Automated, high-throughput DNA extraction protocol for disposable label-free microfluidics integrating DNA biosensor for oil palm pathogen, Ganoderma boninense," *Process Biochemistry*, vol. 92, no. January, pp. 447–456, May 2020, doi: 10.1016/j.procbio.2020.02.003.

[11] A. Josephin *et al.*, "Easy extraction of Ganoderma boninense liquid sample using portable on-chip device," *Indones J Biotechnol*, vol. 29, no. 1, p. 33, Mar. 2024, doi: 10.22146/ijbiotech.83645.

[12] Y.-H. Cheng, C.-H. Wang, K.-F. Hsu, and G.-B. Lee, "Integrated Microfluidic System for Cell-Free DNA Extraction from Plasma for Mutant Gene Detection and Quantification," *Anal Chem*, vol. 94, no. 10, pp. 4311–4318, Mar. 2022, doi: 10.1021/acs.analchem.1c04988.

[13] B. Xiao *et al.*, "Integrating microneedle DNA extraction to hand-held microfluidic colorimetric LAMP chip system for meat adulteration detection," *Food Chem*, vol. 411, p. 135508, Jun. 2023, doi: 10.1016/j.foodchem.2023.135508.

[14] Y. Xie *et al.*, "An open source, PCR-based, point-of-care testing platform," *Sci Rep*, vol. 15, no. 1, p. 12025, Apr. 2025, doi: 10.1038/s41598-025-95639-x.

[15] L. Zhang *et al.*, "Portable DNA extraction integrated with LAMP-CRISPR/Cas12a technology for on-site detection of Salmonella Typhimurium," *NPJ Sci Food*, vol. 9, no. 1, p. 39, Mar. 2025, doi: 10.1038/s41538-025-00401-2.

[16] T. J. Saville *et al.*, "Microfluidic qPCR for detection of 21 common respiratory viruses in children with influenza-like illness," *Sci Rep*, vol. 14, no. 1, p. 28292, Nov. 2024, doi: 10.1038/s41598-024-79407-x.

[17] A. Sun *et al.*, "An integrated microfluidic platform for nucleic acid testing," *Microsyst Nanoeng*, vol. 10, no. 1, p. 66, May 2024, doi: 10.1038/s41378-024-00677-6.

[18] A. Joesaar *et al.*, "A microfluidic platform for extraction and analysis of bacterial genomic DNA," *Lab Chip*, vol. 25, no. 7, pp. 1767–1775, 2025, doi: 10.1039/D4LC00839A.

[19] C. Ianniello, J. Sero, D. Gough, B. Kasprzyk-Hordern, and N. M. Reis, "DNA extraction from bacteria using a gravity-driven microcapillary siphon," *Lab Chip*, 2025, doi: 10.1039/D4LC00735B.

[20] M. Xiong *et al.*, "Space-coded microchip for multiplexed respiratory virus detection via CRISPR-Cas12a and RPA," *Talanta*, vol. 291, p. 127815, Aug. 2025, doi: 10.1016/j.talanta.2025.127815.

[21] A. Ayoib, U. Hashim, M. K. M. K. Arshad, and V. Thivina, "Soft lithography of microfluidics channels using SU-8 mould on glass substrate for low cost fabrication," *IECBES 2016 - IEEE-EMBS Conference on Biomedical Engineering and Sciences*, pp. 226–229, 2016, doi: 10.1109/IECBES.2016.7843447.

[22] A. Ayoib, U. Hashim, S. C. B. Gopinath, V. Thivina, and M. K. M. Arshad, "Design and fabrication of PDMS microfluidics device for rapid and label-free DNA detection," *Applied Physics A*, vol. 126, no. 3, p. 193, Mar. 2020, doi: 10.1007/s00339-020-3337-7.

[23] G. Samla, K. B. Gan, and S.-M. Then, "Modeling microfluidic DNA extraction using superparamagnetic bead particles in COMSOL multiphysics simulation," *Microsystem Technologies*, pp. 1–6, 2016, doi: 10.1007/s00542-016-3170-2.

[24] J. H. Cota-Sánchez, K. Remarchuk, and K. Ubayasena, "Ready-to-use DNA extracted with a CTAB method adapted for herbarium specimens and mucilaginous plant tissue," *Plant Mol Biol Report*, vol. 24, no. 2, pp. 161–167, Jun. 2006, doi: 10.1007/BF02914055.

[25] C. G. Athanasio, J. K. Chipman, M. R. Viant, and L. Mirbahai, "Optimisation of DNA extraction from the crustacean *Daphnia*," *PeerJ*, vol. 4, p. e2004, 2016, doi: 10.7717/peerj.2004.

[26] Y. He *et al.*, "Molecular Interactions for the Curcumin-Polymer Complex with Enhanced Anti-Inflammatory Effects," *Pharmaceutics*, vol. 11, no. 9, p. 442, Sep. 2019, doi: 10.3390/pharmaceutics11090442.

[27] G. Lucena-Aguilar, A. M. Sánchez-López, C. Barberán-Aceituno, J. A. Carrillo-Ávila, J. A. López-Guerrero, and R. Aguilar-Quesada, "DNA Source Selection for Downstream Applications Based on DNA Quality Indicators Analysis," *Biopreserv Biobank*, vol. 14, no. 4, pp. 264–270, Aug. 2016, doi: 10.1089/bio.2015.0064.

[28] N. Rizan, T. Y. Shin, H. A. Tajuddin, G. Gnana Kumar, and V. Periasamy, "Effect of pH on the Conductivity of Basidiomycetes DNAs Integrated Within Schottky-Like Junctions," *ChemistrySelect*, vol. 5, no. 2, pp. 601–609, Jan. 2020, doi: 10.1002/slct.201903643.

[29] G. Yammouri, H. Mohammadi, and A. Amine, "A Highly Sensitive Electrochemical Biosensor Based on Carbon Black and Gold Nanoparticles Modified Pencil Graphite Electrode for microRNA-21 Detection," *Chemistry Africa*, vol. 2, no. 2, pp. 291–300, Jun. 2019, doi: 10.1007/s42250-019-00058-x.

[30] V. Thivina *et al.*, "Distinct Detection of Ganoderma Boninense On Metal Oxides-Gold Nanoparticle Composite Deposited Interdigitated Electrode DNA sensor," *J Phys Conf Ser*, vol. 2129, no. 1, p. 012050, Dec. 2021, doi: 10.1088/1742-6596/2129/1/012050.

[31] H. Moustakim, H. Mohammadi, and A. Amine, "Electrochemical DNA Biosensor Based on Immobilization of a Non-Modified ssDNA Using Phosphoramidate-Bonding Strategy and Pencil Graphite Electrode Modified with AuNPs/CB and Self-Assembled Cysteamine Monolayer," *Sensors*, vol. 22, no. 23, p. 9420, Dec. 2022, doi: 10.3390/s22239420.

[32] A. Ayoib, "Hybrid Nanomaterials in Biosensors for Advanced Point-of-Care Diagnostics: DNA-, Enzyme-, or Immunosensor-Based, for Healthcare," in *Hybrid-Nanomaterials*, 1st ed., S. C. B. Gopinath and M. M. Ramli, Eds., Springer, Singapore, 2024, ch. 7, pp. 123–153. doi: 10.1007/978-981-97-9022-7_7.